HHS Public Access

Author manuscript

Neurobiol Dis. Author manuscript; available in PMC 2016 February 01.

Published in final edited form as:

Neurobiol Dis. 2015 February ; 74: 167–179. doi:10.1016/j.nbd.2014.11.014.

Cumulative mtDNA damage and mutations contribute to the progressive loss of RGCs in a rat model of glaucoma

Ji-hong Wu[#1,2], **Sheng-hai Zhang**[#1,2], **John M. Nickerson**[3], **Feng-juan Gao**[1], **Zhongmou Sun**[4], **Xin-ya Chen**[1], **Shu-jie Zhang**[1], **Feng Gao**[1], **Jun-yi Chen**[1], **Yi Luo**[1], **Yan Wang**[1], and **Xing-huai Sun**[1,2,5,**]

[1]Eye & ENT Hospital, Institutes of Brain Science, Shanghai Medical college, Fudan University, Shanghai 200032, China

[2]Shanghai Key Laboratory of Visual Impairment and Restoration, Shanghai 200032, China

[3] Ophthalmology Department, Emory University, Atlanta, GA, 30322, USA

[4] Wesleyan University, Middletown, CT, 06459, USA.

[5] State Key Laboratory of Medical Neurobiology, Institutes of Brain Science, Shanghai Medical college, Fudan University, Shanghai 200032, China

[#] These authors contributed equally to this work.

Abstract

Glaucoma is a chronic neurodegenerative disease characterized by the progressive loss of retinal ganglion cells (RGCs). Mitochondrial DNA (mtDNA) alterations have been documented as a key component of many neurodegenerative disorders. However, whether mtDNA alterations contribute to the progressive loss of RGCs and the mechanism whereby this phenomenon could occur are poorly understood. We investigated mtDNA alterations in RGCs using a rat model of chronic intraocular hypertension and explored the mechanisms underlying progressive RGC loss. We demonstrate that the mtDNA damage and mutations triggered by intraocular pressure (IOP) elevation are initiating, crucial events in a cascade leading to progressive RGC loss. Damage to and mutation of mtDNA, mitochondrial dysfunction, reduced levels of mtDNA repair/replication enzymes, and elevated reactive oxygen species form a positive feedback loop that produces irreversible mtDNA damage and mutation and contributes to progressive RGC loss, which occurs even after a return to normal IOP. Furthermore, we demonstrate that mtDNA damage and mutations increase the vulnerability of RGCs to elevated IOP and glutamate levels, which are among the most common glaucoma insults. This study suggests that therapeutic approaches that

[**]Corresponding author: Xing-huai Sun, Eye & ENT Hospital, and the State Key Laboratory of Medical Neurobiology, Institutes of Brain Science, Shanghai Medical college, Fudan University, 83# Fenyang Road, Shanghai 200032, China. xhsun@shmu.edu.cn..

Conflict of interest

The authors declare no competing financial interests.

target mtDNA maintenance and repair and that promote energy production may prevent the progressive death of RGCs.

Keywords

retinal ganglion cell; glaucoma; mitochondrial DNA; mutation

Introduction

Glaucoma is a complex, multifactorial neurodegenerative disease (Gupta and Yucel, 2007). Progressive retinal ganglion cell (RGC) death is a primary contributor to the loss of vision, and elevated intraocular pressure (IOP) is a major risk factor (Buckingham et al., 2008; Kwon et al., 2009). Factors known to be involved in glaucoma pathogenesis include mechanical stress due to elevated IOP, axonal transport failure, reduced blood flow to the retina, reperfusion injury, oxidative stress, glutamate excitotoxicity, aberrant immune response, and glial dysfunction (Wax et al., 2008) (Almasieh et al., 2012). However, these factors have not yet provided a plausible explanation for why the adequate control of IOP only delays rather than halts RGC loss and glaucoma progression (Cantor, 2006; Osborne, 2010). An in-depth understanding of the molecular basis of accelerated RGC death, which can occur months or years after the initiation of glaucoma (Osborne, 2010), is critical for the development of new therapeutic strategies for protecting RGCs and the optic nerve in glaucoma patients.

Mitochondrial DNA (mtDNA) damage and mutations have been documented as a key component of many neurodegenerative disorders. mtDNA is much more susceptible than nuclear DNA (nDNA) to damage because of the lack of DNA protection by histones and the proximity to reactive oxygen species (ROS) generated by the mitochondrial respiratory chain (Mambo et al., 2003). Unrepaired DNA damage can result in mutations (Mambo et al., 2003). These alterations (damage and mutations) of the mtDNA can compromise oxidative phosphorylation (DiMauro and Schon, 2003; Pickrell et al., 2011a), ultimately resulting in cell death in many neurodegenerative diseases, including disorders without a primary mitochondrial etiology (Pickrell et al., 2011b; Reeve et al., 2013; Schon et al., 2012; Vives-Bauza and Przedborski, 2011).

RGCs, which are among the most metabolically active and energy-intensive cells in the body, have many mitochondria and are sensitive to primary or secondary mitochondrial abnormalities (Bristow et al., 2002). Many clinical studies have suggested that mitochondrial dysfunction may be involved in glaucoma (Chrysostomou et al., 2013; Osborne and del Olmo-Aguado, 2013; Tezel, 2006). Recent studies have reported an increase in mtDNA mutations and deficiencies in complex I-linked respiration and ATP synthesis in the peripheral blood of primary open-angle glaucoma patients (Abu-Amero et al., 2006; Lee et al., 2012). In addition, mtDNA deletion is frequent in the trabecular meshwork of glaucoma patients (Izzotti et al., 2011). However, little is known about alterations to RGC mtDNA in glaucoma, whether such changes to mtDNA contribute to the progressive loss of RGCs, or the mechanism whereby this could occur.

In the present study, we investigated alterations of mtDNA in RGCs using a well-established rat glaucoma model (Urcola et al., 2006; Wu et al., 2010) and explored the mechanisms underlying the progressive loss of RGCs. We demonstrate that mtDNA alterations caused by elevated IOP are crucial to the progressive loss of RGCs. These alterations include both damage and mutations. Alterations in mtDNA, mitochondrial dysfunction, a reduction in the levels of mtDNA repair/replication enzymes, and ROS form a positive feedback loop that generates irreversible mtDNA alterations and contributes to progressive RGC loss, even after a return to normal IOP. Furthermore, the present study demonstrates that mtDNA alterations increase the susceptibility of RGCs to apoptosis induced by elevated IOP and glutamate levels, which are among the most common insults in glaucoma. Our study implies that therapeutic approaches that target the mitochondria and promote energy production may protect RGCs in glaucoma patients, regardless of cause or etiology.

Materials and methods

Animals

Eight-week-old male Wistar rats (SLAC Laboratory Animal Co. Ltd, Shanghai, China) were housed under constant 12-h light/dark cycles, with access to a standard rodent diet ad libitum. All experiments and animal care procedures adhered to the ARVO (The Association for Research in Vision and Ophthalmology) Statement for the Use of Animals in Ophthalmic and Vision Research and the European Communities Council Directive 2010/63/EU. The animals were randomly divided into 4 treatment groups: (1) glaucomatous model; (2) glaucomatous model with intravitreal injection of AAV2-DNA polymerase gamma (POLG) (AAV2-GFP as a vector control) to prevent mtDNA mutations in RGCs; (3) normal rat with intravitreal injection of AAV2-GFP-shPOLG (AAV2-GFP-shCTL as a vector control) to induce mtDNA mutations in RGCs; and (4) untreated age-matched rats as normal controls. We chose POLG for overexpression in these rat groups because it is the only DNA polymerase known to function in mitochondria that is responsible for mtDNA replication and repair (Suppl Table 1). Mutation or knockdown of the POLG gene results in increased alterations in mtDNA (Tewari et al., 2012; Trifunovic et al., 2005).

At the desired time, the animals were euthanized by an overdose of 10% chloral hydrate, and the retinas were harvested immediately. At each time point, 7 or 8 retinal specimens were pooled to generate each isolated RGC sample. A total of 3 RGC samples (n=22-24 retinas) were obtained and analyzed for each group at each time point. Approximately 10-mm lengths of optic nerves, beginning at the optic nerve head, were collected for histological evaluation of optic nerve axon survival.

Experimental rat glaucoma model

Unilateral IOP elevation was induced by episcleral vein cauterization (EVC) to establish the glaucomatous model, which has been routinely used in our laboratory and has been described previously (Ji et al., 2012; Wu et al., 2010). Briefly, general anesthesia was induced by intraperitoneal injection of 10% chloral hydrate. Three episcleral veins were exposed by making an incision through the conjunctiva and Tenon's capsule at the limbal periphery of the dorsal eye. Cautery was precisely applied to the selected veins. The

contralateral eyes, which served as controls, were sham-operated by isolating the veins in a similar manner without any cauterization. The eyes were treated topically with an antibiotic (Tobrex; Alcon-Couvreur, Belgium) during recovery.

The IOP was measured in both eyes using the TonoLab rebound tonometer for rodents (TioLat, Helsinki, Finland) before surgery (as a baseline), 1 day after surgery, weekly for the subsequent 2 months, and at monthly intervals until 6 months after surgery. The IOP was always measured in the morning under general anesthesia, typically within 2-3 min after the animal lost consciousness and failed to respond to touch. Each IOP was calculated as the mean of the middle 4 readings out of 6 valid rebound measurements. Rats in the cauterized group that did not exhibit an increased IOP of >30% above the baseline within 6 weeks after surgery were excluded from the experiment. The IOP in the cauterized eyes gradually returned to normal by 6 weeks after surgery, and the animals were maintained for an additional 4.5 months.

Generation of AAV2-POLG and AAV2-shPOLG

To construct the AAV2-POLG, the rat POLG gene was synthesized by GenScript and cloned into the pAAV-CMV vector (Stratagene) with AAV2 inverted terminal repeats.

To construct the AAV2-shPOLG, 3 short-hairpin RNAs (shRNAs) directed to different target sites of the *Polg* mRNA (shPOLG1, base pairs 626-654; shPOLG2, base pairs, 1,960-1,988; and shPOLG3, base pairs, 2,623-2,651) were prepared using the pSilencer 1.0_U6 siRNA expression vector (Ambion) based on the rat *Polg* mRNA sequence (GenBank NM_ 053528). A scrambled shRNA that did not have a blocking effect on any mRNA was also made to serve as a control (shCTL). An in vitro screen was performed as described previously (Yang et al., 2009) to identify the optimal shRNA construct. Briefly, the shRNA expression plasmid was transfected into AAV-293 cells (Stratagene) using Lipofectamine 2000. At 72 h after transfection, total RNA was isolated to determine the *Polg* mRNA expression by real-time polymerase chain reaction (PCR), revealing that shPOLG3 was the most effective shPOLG sequence. The DNA containing this shRNA sequence and the U6 promoter was then excised from the shPOLG3 or the shCTL plasmid and cloned into the pAAV-CMV-GFP vector (Stratagene), flanked by AAV2 inverted terminal repeats.

The AAV2-GFP-shPOLG, AAV2-GFP-shCTL, AAV2-GFP, and AAV2-POLG production (AAV Helper-Free kit, Stratagene) and purification (ViraTrap AAV purification kit, GeneMega) were performed using standard methods according to the manufacturer's protocols. The AAV2 titers were determined by real-time PCR as described previously (Olson et al., 2006).

Intravitreal injection of AAV2-POLG and AAV2-shPOLG

To reduce mtDNA mutations in RGCs of the glaucomatous rat, 2 μl of AAV2-POLG or AAV2-GFP (1×10^9 vector genomes/μl, vg/μl) was injected intravitreally 1 week before EVC.

To induce mtDNA mutations in RGCs, normal rats (8 weeks old) received a 2 μl intravitreal injection of AAV2–shPOLG (1×10^9 vg/μl) in the right eye to prevent the normal repair of potential mtDNA mutations; 2 μl of AAV2–shCTL (1×10^9 vg/μl) was injected into the left eye as a contralateral control. The rats were then raised for 12 months to permit the induction of mtDNA mutations and damage in the RGCs; the IOP was measured monthly after the injection. Seven days before euthanasia, either the AAV2-transfected rats or the age-matched controls were randomly assigned to 2 groups (for a total of 4 groups). One group received an intravitreal injection of 2 μl of 4 mM glutamate, as described previously (Finlayson and Iezzi, 2010), while the other group received EVC to induce IOP elevation. The four resulting groups were as follows: (1) AAV2-transfected rats with injection of glutamate; (2) AAV2-transfected rats with EVC; (3) age-matched controls with injection of glutamate; and (4) age-matched controls with EVC. In these experiments, glutamate and IOP elevation were used as secondary insults to evaluate the vulnerability of RGCs that had already experienced mtDNA mutations.

Retrograde labeling of RGCs

RGCs were retrogradely labeled by injecting a solution of DiI fluorescent tracer (Molecular Probes) or Fluoro-Gold (FG, Sigma) into the superior colliculus 3 or 7 days before euthanasia, as described previously (Wu et al., 2010). At euthanasia, the eyes were enucleated, and the retinas were prepared as flat mounts. RGC counts were performed, as previously described (Wu et al., 2010). Cell counting was performed independently by 3 observers in a double-blinded fashion. The data are expressed as the relative percentage of RGC loss in the experimental eye compared with that in the contralateral control.

Histological assessment of the survival of optic nerve axons

The optic nerves were fixed in 2.5% glutaraldehyde with 4% paraformaldehyde in 0.1 M phosphate buffer (pH 7.4) for 24 h, postfixed in 1% osmium tetroxide overnight, and then embedded in epoxy resin (TAAB Laboratories). Semi-thin (0.75 μm) sections 1-1.5 mm from the optic nerve head were cut on a Leica RM2265 microtome, stained with 1% toluidine blue, and examined with a light microscope (Leica). Axonal counting was performed using ImageJ software (NIH, Bethesda, MD, USA).

RGC isolation

RGC isolation was performed with magnetic beads as described previously (Munemasa et al., 2010; Tezel and Wax, 2000). Briefly, retinas isolated from rats were digested, and the cells were collected by centrifugation and resuspended in DPBS containing 0.1% BSA. Macrophages and adherent cells were removed by attachment to CD11b/c monoclonal antibody-coated beads (BD Pharmingen), and RGCs were further purified using magnetic beads that had been coated with Thy-1 monoclonal antibody (Chemicon). The purity of the isolated RGCs was examined by TUJ-1 immunofluorescence. Approximately 5×10^4-1.2×10^5 isolated RGCs were obtained from one retina, and the RGCs from 7-8 retinas were pooled into one isolated RGC sample (3.5×10^5-9.6×10^5 isolated RGCs) in each experiment.

Mitochondria isolation

A Mitochondria Isolation Kit (Pierce) was used to isolate mitochondria, as previously reported (Zhang et al., 2010). Intact mitochondria were separated from the freshly isolated RGCs by differential centrifugation according to the manufacturer's protocol. These preparations were relatively free of other subcellular contaminants (Santos et al., 2011; Tewari et al., 2012). The isolated mitochondrial pellet was resuspended in 100 μl of 210 mM mannitol, 70 mM sucrose, 5 mM HEPES, 1 mM EGTA, and 0.5% (w/v) fatty-acid-free BSA solution.

Western blot analysis

Total proteins from the isolated RGCs were extracted using cell lysis buffer (Cell Signaling Technology) supplemented with a protease inhibitor cocktail (Sigma-Aldrich). The protein concentrations were determined with a BCA protein assay kit (Pierce). Each protein preparation (15-20 μg) was separated by SDS-PAGE and electrotransferred to a polyvinylidene difluoride membrane, which was blocked with 5% nonfat milk for 20 min. The membranes were incubated with primary antibodies against 8-oxoguanine DNA glycosylase (OGG1, Abcam), MutY homolog (MYH, Abcam), DNA polymerase gamma (POLG, Abcam), cleaved caspase-3 antibody (5A1, Cell Signaling), cytochrome b (CYTB, Santa Cruz Biotechnology), ND4 (Santa Cruz Biotechnology), ND5 (Bioss, Inc.), and ND6 (Bioss, Inc.) (Suppl Table 1). The loading controls were β-actin (Sigma) for total protein and Cox IV (Molecular Probes) for mitochondria. The secondary antibodies were HRP-conjugated goat anti-rabbit antibody and HRP-conjugated goat anti-mouse antibody (Millipore). The resulting western blots were exposed to film (Hyperfilm ECL, Amersham Pharmacia Biotech), and images of these films were captured using the Kodak Imaging System (Kodak 440CF). The band intensity was determined by densitometry using ImageJ software (NIH, Bethesda, MD, USA).

DNA isolation

Total DNA was extracted from the isolated RGCs with a DNeasy blood and tissue kit (QIAGEN) according to the manufacturer's protocol. For the mtDNA, the isolated mitochondria were lysed in the presence of 0.5% SDS and 0.2 mg/ml proteinase K in a solution of 10 mM Tris-HCl, 0.15 M NaCl, and 5 mM EDTA, as reported previously. The mtDNA was purified by phenol/chloroform extraction and ethanol precipitation. The DNA was quantified using the Quant-iT dsDNA assay (Invitrogen).

Quantitation of mtDNA

To quantify the amount of mtDNA present per nuclear genome, we designed mtDNA primers (cytochrome b, cytB) and nDNA primers (β-actin) (Suppl Table 2), and we quantified the mtDNA and nDNA genome by real-time PCR (Applied Biosystems, 7500 Fast), as previously described (Tewari et al., 2012). The thermal conditions were 10 min at 95 °C, followed by 40 cycles of 15 s at 95 °C and 60 s at 60 °C. Each reaction was performed in duplicate using 10 ng of DNA and 10 pmol of each primer. A relative quantification was performed using a SYBR® Premix EX Taq™ kit (TAKARA), and the mtDNA copy number was normalized for variation in the nDNA amount per sample using

the $\Delta\Delta C_t$ method. Absolute quantitation was performed using a TaqMan Universal Master Mix (Applied Biosystems, CA, USA), and the standard curve was generated using ten-fold serial diluted standard plasmid. The amount of each DNA copy number was calculated from the standard curve. The two methods yielded identical results.

Mitochondrial DNA mutation assays

Random mutation capture assays were performed, as previously described (Chen et al., 2010; Vermulst et al., 2008). The mtDNA was probed with primers flanking the TaqI restriction site to quantify mtDNA molecules containing a mutation in the TaqI restriction site. A second pair of primers that anneal adjacent to the restriction site was used to quantify the mtDNA in the sample. Quantitative PCR was performed in 25-μl reactions containing Brilliant SYBR Green I master mix (Stratagene), 2 μl of 10 μM forward and reverse primers, and 0.2 μl of uracil DNA glycosylase (New England Biolabs, Inc.). The PCR steps were as follows: step 1, 37 °C for 10 min; step 2, 95 °C for 10 min; step 3, 95 °C for 30 s; step 4, 60 °C for 1 min; step 5, 72 °C for 1.5 min; step 6, repeat steps 3-5 44 times; step 7, 72 °C for 5 min; step 8, melting curve from 65 °C to 95 °C; and step 9, hold at 4 °C indefinitely. The primers used for the DNA amplification included the mtDNA primers flanking the TaqI sites at positions 1,427 and 8,335 and the mtDNA control primers (Suppl Table 2). To verify the presence of mtDNA mutations, every PCR product was digested with TaqI, followed by size analysis by gel electrophoresis; mutations were further confirmed by sequencing. The ratio of mutant molecules to the total number of molecules was used to calculate the mutation frequency per base pair, as described previously (Vermulst et al., 2008). The mutation level is expressed as the number of mutations per million bases.

Mitochondrial and nuclear DNA damage

The DNA damage was evaluated either by amplifying long and short regions of mtDNA or nDNA using long-extension (LX)-PCR or by relative quantitation of long and short fragments using real-time PCR (7500 Fast , Applied Biosystems). LX-PCR was performed with the GeneAmp XL PCR kit (Applied Biosystems), as described previously (Santos et al., 2006; Wang et al., 2010). Briefly, 10 ng of DNA was amplified in a reaction mixture containing 1× XL PCR buffer II, 200 μM dNTPs, 1.1 mM Mg $(OAc)_2$, 1 U rTth DNA polymerase, and 0.1 μM gene-specific primers. The 4 pairs of PCR primers employed in this study are given in Suppl Table 2. The PCR thermocycler program for the mtDNA long product was 94 °C for 1 min, followed by 24 cycles of 94 °C for 15 s, 65 °C for 12 min, and 72 °C for 12 min; the program for the mtDNA short product was 94 °C for 1 min, followed by 18 cycles of 94 °C for 15 s, 65 °C for 12 min, and 60 °C for 12 min. The PCR thermocycler program for the nDNA long product was 94 °C for 1 min, followed by 28 cycles of 94 °C for 15 s, 65 °C for 12 min, and 72 °C for 12 min. The same program was used for the short nDNA product, except that the extension temperature was 60 °C. The DNA damage was assessed by measuring the band intensity of the PCR gel photographs using Un-Scan-It Gel 6.0 digitizing software and quantifying the ratio of the long and short fragments of the PCR amplicons (mtDNA=13.4 kb/235 bp, nDNA=12.5 kb/195 bp). Real-time PCR was conducted using SYBR® Premix Ex Taq™ (TaKaRa)to further determine the amount of long and short fragment in the same amount of mtDNA/nDNA. The primers were

the same as the above. The mtDNA/nDNA damage was indicated by the ratio of the amount of long and short fragments.

RNA isolation and quantitative PCR

Total RNA from the isolated RGCs was extracted using Trizol reagent (Invitrogen), purified using RNeasy mini-columns (QIAGEN), and treated with RNase-free DNase I (QIAGEN). The RNA purity was verified by confirming that the $OD_{260\ nm}/OD_{280\ nm}$ ratio exceeded 1.9. cDNA was synthesized using the SuperScript II first-strand RT-PCR kit (Invitrogen). The gene expression of *Polg*, *Ogg1*, *Myh*, *ND4*, *ND5*, *ND6*, and *CytB* was measured by SYBR Green-based real-time PCR (Applied Biosystems, 7500 Fast). The primers for each gene of interest were designed for each target mRNA and are shown in Suppl Table 2. The β-actin gene was used as a normalization control. All qRT-PCR reactions used 40 ng of cDNA. The reactions were performed in duplicate in 2 separate experiments, and the transcripts were quantified using the $\Delta\Delta C_t$ method.

Mitochondrial function assay

The mitochondrial complex I and III (Suppl Table 1) activities were measured, as reported previously (Rosca et al., 2005; Yao et al., 2011).

The ATP production rate (Suppl Table 1) was measured with a standard bioluminescence assay kit (ENLITEN ATP assay system; Promega) according to the manufacturer's protocol. Briefly, the mitochondrial pellet was resuspended in hypotonic solution, as described above. The ENLITEN rL/L Reagent dissolved in sample buffer was injected immediately before the results were read, and the ATP concentrations were determined with a BioTek Synergy HT microplate reader and normalized to total mitochondrial protein. The data are presented as the averages of 3 independent experiments assayed in duplicate.

The ROS (Suppl Table 1) production was determined using an OxiSelect ROS Assay Kit (Cell Biolabs, Inc.) according to the manufacturer's instructions. Briefly, a 100-μl suspension of isolated RGCs (1×10^5 cells) was mixed with 100 μl of a 1× solution of 2',7'-dichlorofluorescein-diacetate (DCFH-DA) and incubated for 1 h. The cells were lysed according to the manufacturer's specifications, and the 2', 7'-dichlorofluorescein (DCF) fluorescence was measured using a BioTek Synergy HT microplate reader. The values are presented in arbitrary units.

Immunofluorescence staining and terminal deoxynucleotidyl transferase dUTP nick end-labeling (TUNEL) assay

Rats in which RGC mtDNA alterations were induced were euthanized at the indicated time after receiving AAV2-shPOLG intravitreal injections. The eyes were enucleated and fixed in 4% paraformaldehyde for 4 h, and 8-μm-thick sections were obtained using a cryostat (Leica CM 3050S). Immunofluorescence staining was performed using the primary antibody against POLG (Abcam) and the secondary antibody Cy5-conjugated anti-rabbit IgG (Molecular Probes), as described previously (Wu et al., 2010). For the TUNEL assay, an in situ cell death detection kit (TMR Red, Roche) was used to label apoptotic cells according to

the manufacturer's instructions. The sections were observed with a confocal microscope (Leica).

Statistical analysis

The statistical analysis was performed using SigmaStat software. The data are expressed as the means ± SEM. The Shapiro-Wilk test was used to determine whether the data were normally distributed. For variables that were normally distributed, the data were analyzed by analysis of variance followed by the Bonferroni test. Findings with p values of less than 0.05 were considered statistically significant.

Results

RGC degeneration after high IOP

EVC induced a sustained elevation in IOP, as previously reported (Wu et al., 2010). In this study, the EVC eyes exhibited elevated IOP at 1 day after surgery, and in 60% of EVC-treated cases, the IOP remained elevated for 6 weeks (22.12±2.31 mmHg). In these cases, the IOP gradually returned to normal by 7 weeks after EVC due to vascular recanalization (Fig. 1A). The IOP in the contralateral eye with the sham operation was approximately 12.16±0.89 mmHg throughout the experiments (Fig. 1A). We previously reported a significant loss of RGCs at 2 and 4 weeks after EVC due to IOP elevation (Wu et al., 2010). Here, we determined if a further loss of RGCs occurs after return of the elevated IOP to normal levels. The numbers of intact FG-labeled RGCs in the EVC eyes were 21.9±1.24% ($p < 0.05$) and 41.7±2.26% ($p < 0.01$) lower than those in the contralateral control eyes with sham-operated treatment at 6 weeks and 6 months, respectively (Fig. 1B, C, Suppl Fig.1). As expected, the number of axons in the cross-sections through the optic nerve, indicated by toluidine blue staining, decreased by over 34% from 6 weeks to 6 months after EVC (Fig. 1D). We found that the number of RGCs or their axons was obviously diminished at 6 months compared to 6 weeks after EVC, suggesting the RGC loss occurred not only during IOP elevation (within 6 weeks after EVC) but also during the reversal of IOP elevation between 6 weeks and 6 months. Together, these results demonstrate the progressive loss of RGCs and their axons in EVC-treated eyes, even after the IOP has returned to normal levels, which is consistent with the clinical features of primary open-angle glaucoma (Kwon et al., 2009).

mtDNA changes after high IOP

Given the features of RGC loss after the return of elevated IOP to normal levels and the crucial role of the mitochondria in cell death, we first determined if any mtDNA alterations occurred in the RGCs of EVC eyes. Consistent with previous reports (Munemasa et al., 2008; Tezel and Wax, 2000), > 95% of the isolated RGCs cells were positive for TUJ-1 (data not shown). As shown in Figure 2A, although IOP-elevation-induced mtDNA damage (indicated by the ratio of 13.4 kb and the 235 bp mtDNA band) was observed in RGCs beginning 2 weeks after EVC and cumulatively increased, no significant damage was observed at 6 weeks. A significant increase in mtDNA damage was detected at 2 months. Surprisingly, the damage continued to increase thereafter ($p<0.05$ when the mtDNA damage of 2, 4 and 6 months after EVC compared each other), although IOP had already dropped to

normal levels, reaching 3.4-fold ($p<0.01$) more damage compared to the RGCs from the contralateral eye at 6 months (Fig. 2A, right). This result was further confirmed by quantitation of the long and short fragments using real-time PCR (Suppl Fig. 2). In contrast, there was no significant difference in nDNA damage from RGCs of the EVC and contralateral sham-operated eye at either 6 weeks or 6 months (Fig. 2B).

Next, we examined the frequency of mtDNA mutations in the RGCs by random mutation capture assay. The RGCs from the EVC eyes harbored 5.6-fold ($p<0.05$) more mutations in mtDNA compared with the contralateral control at 6 weeks after EVC. The mutations continued to accumulate, although the IOP had returned to normal, and reached 16.8-fold more mutations than the sham-operated contralateral eye ($p<0.01$) at 6 months, at which time the experiment was terminated (Fig. 2C). We confirmed this measurement by interrogating one additional locus in the mitochondrial genome (Fig. 2D).

To determine if any changes in the abundance of mtDNA occurred within the EVC-treated eyes, we analyzed the mtDNA copy number per nuclear genome in the RGCs. We observed a sharp decrease in the mtDNA copy number in the RGCs at 1 week after IOP elevation compared with the RGCs from control retinas (a decrease of 52.3%, $p<0.01$). The progressive reduction in the mtDNA copy number did not reverse when the IOP returned to normal, and the copy number decreased by 49.1% at 6 months after EVC (Fig. 2E).

DNA repair and replication compromise after IOP elevation

To investigate the capacity to repair mtDNA damage and replicate mtDNA, we quantified the mRNA and protein expression of the DNA glycosylases OGG1 and MYH, which recognize and remove altered bases, and POLG, an enzyme responsible for the replication/repair of mtDNA. One week after EVC, the mRNA levels of OGG1 and MYH in the isolated RGCs sharply increased by 18.9-fold ($p<0.01$) and 8.5-fold ($p<0.01$), respectively, relative to the contralateral sham-operated eyes. Subsequently, the mRNA expression of both genes gradually dropped but remained slightly elevated compared with the control eyes until 6 months after EVC (Fig. 3A). In contrast, despite similar CoxIV expression in the mitochondria obtained from the EVC eyes and controls, the protein levels of OGG1 and MYH decreased by 12-21% and 8-46%, respectively, when IOP was elevated, except for the slightly increased OGG1 protein levels 1 week after EVC. Importantly, these levels remained reduced from 6 weeks to 6 months after EVC, even when the IOP returned to normal (Fig. 3B). Further evidence was obtained by western blot analysis of OGG1 and MYH levels in the nucleus and in isolated mitochondria at 6 months after EVC (Fig. 3C). The *POLG* mRNA was increased 1.8-fold ($p<0.05$) at 2 weeks after EVC and gradually dropped to subnormal levels at 6 weeks. At 6 months after EVC, the *POLG* mRNA was decreased by 48% (Fig. 3A). The mitochondrial accumulation of the POLG protein was consistent with its gene expression and decreased by more than 50% at 6 months (Fig. 3B). The reduction in mtDNA repair and replication enzymes from 6 weeks to 6 months after EVC indicates that irreversible impairment of the DNA repair and replication capacity occurs after high IOP, which may result in further long-term, sustained mtDNA damage and mutation, even after the return of normal IOP.

Accelerated mitochondrial dysfunction in RGCs of EVC eyes

RGCs, which are among the most metabolically active cells in the body, contain many mitochondria, on which they are heavily dependent for their proper function (Bristow et al., 2002). Oxidative stress occurs in the retina at an early stage in experimental glaucoma models (Ko et al., 2005; Moreno et al., 2004; Tezel, 2006). However, the status and mechanisms of the underlying mitochondrial function remain unclear. Here, we investigated whether and how the cumulative, irreversible mtDNA alterations after high IOP lead to mitochondrial dysfunction in RGCs. First, we assessed the dynamic changes in the respiratory chain complex activity in RGCs isolated from EVC eyes when the IOP was elevated and once it had returned to normal levels. As shown in Figure 4A, a significant reduction (36% reduction, $p<0.05$) in complex I activity was detected 6 weeks after EVC. After the IOP had returned to normal, complex I activity remained below normal from 6 weeks to 6 months. In contrast to complex I, complex III activity declined as early as 2 weeks after EVC and continued to decrease until the experiment was terminated (reduction of 61% at 6 months, $p<0.01$) (Fig. 4B). To further characterize the possible mechanisms of complex activity impairment, we examined the protein levels of the mtDNA-encoded ND4, ND5, and ND6 subunits of complex I and cytochrome b of complex III. Western blot analysis revealed a significant decrease in cytochrome b, ND5, and DN6 in the mitochondria isolated from the RGCs of EVC eyes (Fig. 4C), suggesting that the reduction in the activity of these 2 complexes might be due to the decreased expression of mtDNA-encoded proteins. In addition, no detectable alteration in ND4 was observed (Fig. 4C), suggesting that not all mtDNA-encoded proteins were affected by mtDNA mutations and damage from IOP elevation.

Respiratory chain complex I and III activities are closely related to energy production, which is the foremost indicator of mitochondrial function. We measured the mitochondrial ATP production rate (MAPR) of RGCs isolated from EVC eyes. Considerably increased MAPRs that were 3.6- to 5.3-fold ($p<0.01$) higher than those in the sham-operated contralateral eyes were detected within 2 weeks of EVC, coincident with the onset of IOP elevation, suggesting that increased MAPR may be a compensatory response of mitochondria to pressure stress. Subsequently, the MAPR gradually dropped, and the reduction did not halt despite a return of the IOP to normal levels. The MAPR was decreased by 27% at 6 months after EVC ($p<0.05$; Fig. 4D).

ROS production is another important index of mitochondrial function. We found that ROS levels were significantly elevated by 46% ($p<0.05$) as early as 1 week after EVC and returned to the normal range at 2-6 weeks after EVC, when the IOP was still elevated. This result is consistent with a previous report regarding dynamic ROS changes in retinas experiencing elevated IOP (Moreno et al., 2004). Interestingly, we observed a second elevation in the ROS levels 2 months after EVC, when the IOP had returned to normal. The values gradually increased thereafter (Fig. 4E), suggesting that progressive mitochondrial dysfunction rather than an elevated IOP may contribute to the secondary increase in ROS, forming a positive feedback cycle of mtDNA damage and mitochondrial dysfunction. In summary, we found accelerated decreases in complex activities, decreases in MAPR, and increases in ROS in RGCs from 6 weeks to 6 months after EVC. These changes may suggest

that irreversible mitochondrial dysfunction contributes to progressive RGC loss, especially after the IOP returns to normal.

Preventing mtDNA alterations improves RGC survival

We hypothesized that prevention of mtDNA damage and mutations can improve RGC survival after IOP elevation. To test this hypothesis, we asked if overexpression of POLG, a key enzyme in mtDNA replication/repair that is significantly decreased after IOP, would reduce mtDNA alterations from EVC-stressed RGCs. We intravitreally injected AAV2-POLG/GFP 1 week before EVC and then examined the mtDNA alterations in RGCs and the loss of RGCs and their axons. We reported previously that AAV2 could efficiently transduce exogenous genes in RGCs and maintain the expression of these genes for more than 1 year (Zhang et al., 2008). In this study, as shown in Figure 5A, *POLG* mRNA increased by 6.5-12.4-fold in the RGCs of the EVC eyes injected with AAV2-POLG compared to the EVC eyes injected with the control, AAV2-GFP. Western blotting confirmed that the POLG protein levels in the mitochondria of the RGCs were increased in the EVC eyes injected with AAV2-POLG compared to those injected with AAV2-GFP (Fig. 5B).

POLG is the only DNA polymerase found in the mitochondria that mediates DNA replication and repair. To test whether the over-expressed POLG was functional in reducing mtDNA alterations, we assayed the mtDNA damage and mutation rate in the RGCs of EVC eyes. The mtDNA damage (indicated by the ratio of 13.4 kb/210 bp fragments) was reduced by 13.04% and 43.5% ($p < 0.05$) at 6 weeks and 6 months, respectively, comparing AAV2-POLG expressed in EVC eyes versus control AAV2-GFP expression (Fig. 5C). Next, using the random mutation capture assay, the mutation rates at either the 1,427 or 8,335 site of the mitochondrial genome were measured (Fig. 5D), and AAV2-POLG injections reduced these mutation rates compared to control AAV2-GFP injections.

Further, POLG overexpression (compared to control GFP expression) significantly improved the mitochondrial complex I and III activities in the RGCs from the EVC eyes (Fig. 5E, F). Although the mtDNA alterations and complex activities in the EVC eyes with AAV2-POLG were lower than those of eyes that were not cauterized throughout the experiment, the POLG-treated EVC eyes were markedly more normal than the EVC eyes without POLG treatment (Figs. 5C, D, E and F). These findings suggest that overexpression of POLG itself could partially, but not completely, reduce mitochondrial disorders caused by IOP elevation.

Next, we investigated RGC survival in the EVC eyes after POLG overexpression. As shown in Figure 5G, the numbers of DiI-labeled RGCs in the EVC eyes with AAV2-POLG were 9.5% ± 0.86%, 15% ± 2.58%, and 25.5 ± 4.23% ($p < 0.05$ for each) higher than those in the EVC eyes with AAV2-GFP at 6 weeks, 4 months and 6 months, respectively. Toluidine blue staining showed that the amount of stained axons in the optic nerve was 40% ($p < 0.05$) greater at 6 months in the EVC eyes treated with AAV2-POLG compared to those treated with AAV2-GFP (Fig. 5H). These results indicated that the prevention of mtDNA alterations substantially improved RGC and axon survival in the EVC eyes, especially in the period when IOP had returned to the normal level (6 weeks to 6 months after EVC).

RGC susceptibility to apoptosis

We hypothesized that RGCs bearing more mtDNA sequence alterations are more vulnerable to stresses caused by elevated IOP. To test this hypothesis, we reduced the POLG levels in RGC mitochondria and assessed whether these RGCs were more or less sensitive to IOP changes than RGCs with normal levels of POLG. We employed RNAi targeting POLG expression using AAV2-shPOLG vectors that were intravitreally injected. To lower the POLG mRNA levels, we tested three shRNA variants and found that shPOLG-3 produced a robust knockdown effect on POLG mRNA expression relative to that of a control sequence, shCTL, in AAV-293 cells by real-time PCR and western blotting (data not shown). Next, we generated a recombinant AAV-mediated RNAi construct with shPOLG-3 (AAV2-shPOLG) for in the vivo study. The AAV2-shPOLG vector contains mouse U6 promoter-driven shPOLG (or shCTL for AAV2-shCTL, a non-specific RNAi vector that serves as a negative control) and CMV promoter-driven GFP. AAV2-shPOLG or AAV2-shCTL was intravitreally injected into the eyes of normal 8-week-old Wistar rats. We observed that AAV2-shPOLG significantly inhibited POLG expression in the mitochondria of isolated RGCs (Fig. 6A). Immunofluorescence staining of POLG in the retina provided confirmation of this knockdown (Fig. 6A). We further measured the incidence of mtDNA abnormalities in RGCs induced by the knockdown of POLG in vivo. As shown in Figure 6B, the frequency of mtDNA mutations in RGCs from AAV2-shPOLG-injected eyes increased 11.3-fold at 12 months compared with RGCs from AAV2-shCTL-injected eyes or age-matched normal (untreated) rats. These knockdown results are consistent with a previous report regarding POLG knockout mice (Kong et al., 2011; Kujoth et al., 2005; Trifunovic et al., 2004), though the mechanisms of mtDNA mutation induction are not completely the same. The increase in mtDNA damage was assayed by the ratios of long to short mtDNA fragments using LX-PCR (Fig. 6C). We also measured the ROS levels and found no significant differences in RGCs isolated from AAV2-shPOLG-injected eyes and AAV2-shCTL-injected eyes (Fig. 6D), consistent with previous reports of ROS levels in POLG mutant mice (Kujoth et al., 2005; Trifunovic et al., 2005; Kong et al., 2011). Western blotting showed that ND5, ND6 and CytB decreased in the RGCs from AAV2-shPOLG-injected eyes compared to the controls, while ND4 remained undetectable changed (suppl Fig. 3B), which is consistent with results from the glaucomatous rat model. The mRNA expression of *ND5*, *ND6* and *CytB* also significant decreased ($p<0.05$) in the AAV2-shPOLG-injected eyes (suppl Fig. 3A), suggesting that mtDNA alterations could lead to the decline of the complex subunits ND5, ND6, and CytB.

Elevations in IOP and glutamate are the two common insults of the glaucomatous retina (Almasieh et al., 2012; Pascale et al., 2012). Accordingly, we applied each insult to the rat model 12 months after intravitreal injection of AAV2-shPOLG to assess whether RGCs with increased mtDNA alterations were more susceptible to these secondary insults. IOP elevation was induced by EVC, and glutamate was administered by intravitreal injection. At 1 week after the insults, the RGC layer of the AAV2-shPOLG eyes displayed increased apoptosis compared with the AAV2-shCTL eyes, as assessed by a TUNEL assay (Fig. 6E, two lower panels, Fig. 6F). In addition, we observed greater apoptosis in the RGC layer of AAV2-shPOLG eyes compared with the AAV2-shCTL eyes in the absence of any secondary insults (Fig. 6E, upper panel, Fig. 6F). Quantitative analysis of RGC survival

using retrograde DiI-labeling consistently confirmed that the RGC counts were decreased by 19.9% ($p<0.05$), 18.4% ($p<0.05$), and 16.1% ($p<0.05$) in the eyes treated with AAV2-shPOLG alone, AAV2-shPOLG and EVC, and AAV2-shPOLG and glutamate relative to the eyes treated with AAV2-shCTL alone, AAV2-shCTL and EVC, and AAV2-shCTL and glutamate, respectively (Fig. 6H).

In the mitochondrial apoptosis pathway, mitochondrial dysfunction can lead to mitochondrial outer membrane permeabilization and cytochrome c release into the cytosol to activate caspase-3, a key effector protease, by proteolytic cleavage (Green and Kroemer, 2004; Hengartner, 2000). Therefore, we evaluated whether an increased level of cleaved caspase-3 is a feature of RGC apoptosis that is triggered by mtDNA alterations. Cleaved caspase-3 levels were increased by 11.3%, 20.3%, and 22.6% in the cytosolic fractions of RGCs from eyes treated with AAV2-shPOLG, AAV2-shPOLG and EVC, and AAV2-shPOLG and glutamate, respectively, compared with the corresponding controls (Fig. 6G). Together, these findings strongly suggest that the accumulation of mtDNA alterations not only increases the vulnerability of RGCs to secondary insults but also promotes apoptosis.

Discussion

Our data reveal several interesting features of the mechanisms underlying the progressive RGC loss associated with glaucoma.

First, we provided evidence that progressive RGC death occurred after the elevated IOP returned to normal in a rat glaucomatous model. We found that several mitochondrial problems progressively worsened after the IOP was elevated and then returned back to normal. This progression proceeded as follows: a) the mtDNA mutation rates were elevated, and damage continued to accumulate; b) the mitochondrial functions worsened; and c) the mitochondrial repair and replication systems were irreversibly impaired. These mechanisms all occur and continue well after the IOP had returned to normal for an extended period of time.

Second, we proved that the prevention of mtDNA alterations by POLG overexpression improves RGC survival after IOP elevation.

Third, we demonstrated that more mtDNA alterations promote RGC death and increase the susceptibility of RGCs to apoptosis following a secondary IOP elevation or a glutamate insult in vivo. Together, these results strongly suggest that the accumulated mtDNA alterations caused by IOP elevation are important factors in the progressive loss of RGCs and their axons in glaucoma.

RGC loss after transiently high IOP

The pattern of RGC loss after the return of IOP to normal levels has not been previously studied. Most studies have focused directly on the effects of sustained, elevated IOP on the loss of RGCs or their axons (Danias et al., 2006; Laquis et al., 1998; Mittag et al., 2000; Wu et al., 2010). Here, we provide experimental evidence that the progressive loss of RGCs occurs not only during elevated IOP but also 4.5 months after the return of IOP to normal

levels. In the future, it will be important to study whether the duration of the IOP elevation influences the progressive loss of RGCs once IOP returns to normal.

mtDNA alterations and progressive loss of RGCs

Somatic mutations in mtDNA play a key role in the selective neuronal loss associated with neurodegeneration (Beal, 2005; Lu et al., 2004; Melov, 2004; Reeve et al., 2013; Schon et al., 2012), and the damage is postulated to contribute to chronic eye disease (e.g., age-related macular degeneration and diabetic neuropathy) and retinal aging (Barron et al., 2001; Jarrett et al., 2008; Kong et al., 2011; Wang et al., 2010). Proximity to the electron transport chain and a lack of DNA protection by histones increase the vulnerability of mtDNA to damage compared to that of nDNA (Mambo et al., 2003). Several groups have demonstrated that the levels of oxidized bases are 3-10-fold higher in mtDNA than in nDNA (Szczepanowska et al., 2012; Yakes and Van Houten, 1997). To date, more than 270 pathogenic mtDNA mutations have been documented (Schon et al., 2012). mtDNA damage resulting from a short-duration insult can ultimately be repaired; however, a longer-duration insult leads to persistent damage, which can lead to apoptosis (Madsen-Bouterse et al., 2010; Yakes and Van Houten, 1997). The present study demonstrates that mtDNA damage and mutation continue, even after IOP has returned to normal levels (Figs 2A, C, and D), suggesting a prominent role for mtDNA alterations in the progression of glaucoma.

The base excision repair (BER) pathway is one of the most frequently employed pathways for mtDNA damage repair (Bohr and Anson, 1999; LeDoux and Wilson, 2001). The DNA glycosylases OGG1 and MYH perform critical roles in the BER pathway by recognizing and excising damaged or inappropriate bases. OGG1 and MYH each recognize an individual alteration in damaged DNA and do not require cofactors for their activity (Hegde et al., 2008; Schärer and Jiricny, 2001). POLG is one of the essential components of the BER pathway, in which DNA polymerization by POLG is a key step for the repair of mtDNA lesions (Graziewicz et al. , 2006; Chen et al. , 2002). POLG is also the rate-limiting enzyme in BER, and its inactivation or reduction likely increases the buildup of cytotoxic BER pathway intermediates, including single-strand breaks (Liu and Demple, 2010). Retinal aging is associated with a reduction in mtDNA repair enzymes, such as OGG1 and MYH (Wang et al., 2010). Our results demonstrate that the protein levels of OGG1, MYH, and POLG are significantly decreased in the mitochondria of RGCs when IOP is elevated and after it has returned to normal (Fig. 3B, C). Regarding the changes in which POLG mRNA increases at 1 week and then declines at 6 weeks after high IOP, possible mediating factors may include the compensation of POLG for enhancing the replication capacity induced by the decreasing mtDNA numbers 1 week after EVC stress. However, the exact mechanism underlying the changes in the POLG level remains unclear and requires further investigation. Moreover, we observed a disparity between increased *OGG1* and *MYH* mRNA and decreased protein expression, consistent with a previous report for diabetic retinopathy (Madsen-Bouterse et al., 2010). This disparity suggests that although mitochondria attempt to initiate mtDNA repair mechanisms by upregulating the gene expression of nuclear-encoded OGG1 and MYH to counteract the IOP elevation insult, their protein levels in the mitochondria remain irreversibly deficient, even after the IOP returns to normal levels (Fig. 3C). This disparity might be correlated with an abnormal mitochondrial

membrane potential (Δψm) because the membrane potential is crucial for protein import into mitochondria (Szczepanowska et al., 2012). Our unpublished data indicating that Δψm is impaired under high pressure in vitro support this explanation, but the precise mechanism requires further investigation. Together, these observations suggest that a reduction in mtDNA repair and replication capacity contributes to the accumulation of mtDNA alterations.

The mitochondrial genome (Anderson et al., 1981) encodes 13 polypeptides that constitute key components of the electron transport chain complexes and are crucial for oxidative phosphorylation (Wallace, 1999). mtDNA alterations have been suggested to ultimately cause a bioenergetic deficit, typically with a reduction in complex activity, a reduction in ATP generation, and an increase in the generation of ROS in the affected cell (Schon et al., 2012; Szczepanowska et al., 2012). We observed a gradual decrease in complex I and III activity in the RGCs, even after the IOP returned to normal levels. These complexes were deemed representative of the electron transport chain in this study because complex I deficiency is the most common respiratory chain defect (DiMauro and Schon, 2003) and mtDNA-encoded protein cytochrome b is essential for the formation and activity of complex III (Rana et al., 2000). Furthermore, complexes I and III are the major sites of ROS generation (Chen et al., 2003), and the changing patterns of complex III activity matches that of axon loss after IOP elevation, suggesting that (1) axon degeneration after EVC-induced high IOP is closely related to mitochondrial dysfunction, in light of the sufficient number of mitochondria in the axons; and (2) complex III activity may play a crucial role in the mitochondrial dysfunction of the axons in the EVC-induced glaucomatous model. We observed that ATP production increased immediately after IOP elevation and decreased gradually to below normal levels, even though the IOP returned to normal. These results suggest a compensatory capacity of oxidative phosphorylation and an attempt to repair cell injury at the beginning of the insult. Interestingly, our results (Fig. 4E) indicated a second increase in ROS levels when the IOP returned to normal, resulting in a secondary insult to mtDNA. In short, continued mtDNA alterations may result in a perpetual loop: accumulated mtDNA damage and mutations impair mitochondrial function, ROS generation is increased, and ROS induce further mtDNA damage in RGCs.

In this study, we provide evidence that the prevention of mtDNA damage and mutations improves RGC survival after IOP elevation. However, we noted that the RGC survival rate did not reach normal levels, even when mitochondrial pathology was largely prevented. There are two possible reasons. (1). POLG is only one of multiple enzymes involved in mtDNA alterations after high IOP; therefore, mtDNA damage induced by IOP elevation could not be fully prevented by POLG itself. (2). Factors (including activated microglia) other than mtDNA damage may also contribute to persistent RGC loss.

In addition, we found that overexpression of POLG did not reduce mtDNA alterations remarkably before 4 months (especially before 6 weeks) after EVC, as shown in Fig. 5. This result could be explained as follows. During high IOP in the first 6 weeks, multiple detrimental factors, such as mechanical pressure, ischemia and reperfusion, could work together, contributing to mtDNA mutations and damage. Therefore, there was no obvious effect on the prevention of mtDNA alterations by only increasing POLG expression.

However, when the IOP returned to normal levels in the ensuing months, many factors caused by high pressure were gradually alleviated, while POLG expression appeared to become increasingly lower with time (as shown in Fig. 3A and 3B), thus playing a greater role in mtDNA mutations and damage. Accordingly, the overexpression of POLG can significantly decrease mtDNA alterations during this period.

mtDNA alterations result in RGC apoptosis and vulnerability to secondary insults

To examine the hypothesis that more mtDNA alterations lead to RGC apoptosis, we transduced RGCs in vivo with a knockdown vector, AAV-shPOLG, which reduced POLG expression, and then induced mtDNA alterations by blocking mtDNA replication/repair. A systemic *POLG* mutant mouse exhibits mtDNA mutations in many organs, including the brain, liver, heart, and retina (Kong et al., 2011; Kujoth et al., 2005; Trifunovic et al., 2005; Trifunovic et al., 2004). The present study shows that the intravitreal injection of AAV-shPOLG allows more mtDNA mutations and damage to RGCs. RGCs with increased levels of mtDNA abnormalities were more prone than control RGCs (AAV2-shCTL-injected eye) to apoptosis. Increased levels of ROS were not observed in the RGCs with increased mtDNA alterations, suggesting that increased mtDNA mutations and damage lead to RGC apoptosis by mechanisms other than increased oxidative stress. The absence of marked oxidative stress is consistent with previous reports in mice with POLG mutations (Trifunovic et al., 2005).

Importantly, we found that RGCs with increased mtDNA alterations were significantly more vulnerable to a secondary IOP elevation or glutamate insult compared with the control group (Figs. 6F, G, and H). These results imply that fluctuations in the IOP and in glutamate after the first insult exert a greater effect on RGCs during the course of glaucomatous neuropathy.

Conclusions

Our study uncovered a new mechanism underlying the progressive loss of RGCs in glaucoma: mtDNA damage and mutations, reduced mtDNA repair enzyme capacity, bioenergetic dysfunction and accordingly increased ROS generation establish a positive feedback cycle. The cycle leads to cumulative and irreversible mtDNA alterations that ultimately contribute to the progressive loss of RGCs, even after the IOP is adequately controlled. Our work points to therapeutic approaches that target mitochondria and promote energy production to protect RGCs in glaucoma, regardless of etiology.

Supplementary Material

Refer to Web version on PubMed Central for supplementary material.

Acknowledgments

This study was supported by the Funds for International Cooperation and Exchange of the National Natural Science Foundation of China (Grant No. 81020108017), National Key Basic Research Program of China (2013CB967503), National Natural Science Foundation of China (NSFC81470625, NSFC81470624, NSFC81100636, NSFC81470623), the Shanghai Natural Science Foundation (14ZR1405500), Research to Prevent Blindness, Inc., R01EY016470, P30EY006360.

Abbreviations

mtDNA	mitochondrial DNA
POLG	DNA polymerase gamma
OGG1	8-oxoguanine DNA glycosylase
MYH	DNA glycosylase MutY homolog
ND4	NADH dehydrogenase subunit 4
ND5	NADH dehydrogenase subunit 5
ND6	NADH dehydrogenase subunit 6
cytB	cytochrome b
MAPR	mitochondrial ATP production rate
ROS	reactive oxygen species
EVC	episcleral vein cauterization
shRNAs	short-hairpin RNAs
PCR	polymerase chain reaction
LX-PCR	long-extension PCR
FG	Fluoro-Gold
DPBS	Dulbecco's phosphate-buffered saline
BSA	bovine serum albumin
TUNEL	terminal deoxynucleotidyl transferase dUTP nick end labeling

References

Abu-Amero KK, et al. Mitochondrial abnormalities in patients with primary open-angle glaucoma. Invest Ophthalmol Vis Sci. 2006; 47:2533–41. [PubMed: 16723467]

Almasieh M, et al. The molecular basis of retinal ganglion cell death in glaucoma. Prog Retin Eye Res. 2012; 31:152–81. [PubMed: 22155051]

Anderson S, et al. Sequence and organization of the human mitochondrial genome. Nature. 1981; 290:457–65. [PubMed: 7219534]

Barron MJ, et al. Mitochondrial abnormalities in ageing macular photoreceptors. Invest Ophthalmol Vis Sci. 2001; 42:3016–22. [PubMed: 11687550]

Beal MF. Mitochondria take center stage in aging and neurodegeneration. Ann Neurol. 2005; 58:495–505. [PubMed: 16178023]

Bohr VA, Anson RM. Mitochondrial DNA repair pathways. J Bioenerg Biomembr. 1999; 31:391–8. [PubMed: 10665528]

Bristow EA, et al. The distribution of mitochondrial activity in relation to optic nerve structure. Arch Ophthalmol. 2002; 120:791–6. [PubMed: 12049585]

Buckingham BP, et al. Progressive ganglion cell degeneration precedes neuronal loss in a mouse model of glaucoma. J Neurosci. 2008; 28:2735–44. [PubMed: 18337403]

Cantor LB. Brimonidine in the treatment of glaucoma and ocular hypertension. Ther Clin Risk Manag. 2006; 2:337–46. [PubMed: 18360646]

Carelli V, et al. Retinal ganglion cell neurodegeneration in mitochondrial inherited disorders. Biochim Biophys Acta. 2009; 1787:518–28. [PubMed: 19268652]

Chen D, et al. Age-dependent decline of DNA repair activity for oxidative lesions in rat brain mitochondria. J Neurochem. 2002; 81:1273–84. [PubMed: 12068075]

Chen H, et al. Mitochondrial fusion is required for mtDNA stability in skeletal muscle and tolerance of mtDNA mutations. Cell. 2010; 141:280–9. [PubMed: 20403324]

Chen Q, et al. Production of reactive oxygen species by mitochondria: central role of complex III. J Biol Chem. 2003; 278:36027–31. [PubMed: 12840017]

Chrysostomou V, et al. Oxidative stress and mitochondrial dysfunction in glaucoma. Curr Opin Pharmacol. 2013; 13:12–5. [PubMed: 23069478]

Danias J, et al. Characterization of retinal damage in the episcleral vein cauterization rat glaucoma model. Exp Eye Res. 2006; 82:219–28. [PubMed: 16109406]

DiMauro S, Schon EA. Mitochondrial respiratory-chain diseases. N Engl J Med. 2003; 348:2656–68. [PubMed: 12826641]

Finlayson PG, Iezzi R. Glutamate stimulation of retinal ganglion cells in normal and s334ter-4 rat retinas: a candidate for a neurotransmitter-based retinal prosthesis. Invest Ophthalmol Vis Sci. 2010; 51:3619–28. [PubMed: 20164453]

Graziewicz MA, et al. DNA polymerase gamma in mitochondrial DNA replication and repair. Chem Rev. 2006; 106:383–405. [PubMed: 16464011]

Green DR, Kroemer G. The pathophysiology of mitochondrial cell death. Science. 2004; 305:626–9. [PubMed: 15286356]

Gupta N, Yucel YH. Glaucoma as a neurodegenerative disease. Curr Opin Ophthalmol. 2007; 18:110–4. [PubMed: 17301611]

Hedge ML, et al. Early steps in the DNA base excision/single-strand interruption repair pathway in mammalian cells. Cell Res. 2008; 18:27–47. [PubMed: 18166975]

Hengartner MO. The biochemistry of apoptosis. Nature. 2000; 407:770–6. [PubMed: 11048727]

Humble MM, et al. Polg2 is essential for mammalian embryogenesis and is required for mtDNA maintenance. Hum Mol Genet. 2013; 22:1017–25. [PubMed: 23197651]

Izzotti A, et al. Mitochondrial damage in the trabecular meshwork occurs only in primary open-angle glaucoma and in pseudoexfoliative glaucoma. PLoS One. 2011; 6:e14567. [PubMed: 21283745]

Jarrett SG, et al. Mitochondrial DNA damage and its potential role in retinal degeneration. Prog Retin Eye Res. 2008; 27:596–607. [PubMed: 18848639]

Ji M, et al. Group I mGluR-mediated inhibition of Kir channels contributes to retinal Muller cell gliosis in a rat chronic ocular hypertension model. J Neurosci. 2012; 32:12744–55. [PubMed: 22972998]

Ko ML, et al. Dynamic changes in reactive oxygen species and antioxidant levels in retinas in experimental glaucoma. Free Radic Biol Med. 2005; 39:365–73. [PubMed: 15993335]

Kong YX, et al. Increase in mitochondrial DNA mutations impairs retinal function and renders the retina vulnerable to injury. Aging Cell. 2011; 10:572–83. [PubMed: 21332926]

Kujoth GC, et al. Mitochondrial DNA mutations, oxidative stress, and apoptosis in mammalian aging. Science. 2005; 309:481–4. [PubMed: 16020738]

Kwon YH, et al. Primary open-angle glaucoma. N Engl J Med. 2009; 360:1113–24. [PubMed: 19279343]

Laquis S, et al. The patterns of retinal ganglion cell death in hypertensive eyes. Brain Res. 1998; 784:100–4. [PubMed: 9518569]

LeDoux SP, Wilson GL. Base excision repair of mitochondrial DNA damage in mammalian cells. Prog Nucleic Acid Res Mol Biol. 2001; 68:273–84. [PubMed: 11554303]

Lee S, et al. Impaired complex-I-linked respiration and ATP synthesis in primary open-angle glaucoma patient lymphoblasts. Invest Ophthalmol Vis Sci. 2012; 53:2431–7. [PubMed: 22427588]

Liu P, Demple B. DNA repair in mammalian mitochondria: Much more than we thought? Environ Mol Mutagen. 2010; 51:417–26. [PubMed: 20544882]

Lu T, et al. Gene regulation and DNA damage in the ageing human brain. Nature. 2004; 429:883–91. [PubMed: 15190254]

Madsen-Bouterse SA, et al. Role of mitochondrial DNA damage in the development of diabetic retinopathy, and the metabolic memory phenomenon associated with its progression. Antioxid Redox Signal. 2010; 13:797–805. [PubMed: 20088705]

Mambo E, et al. Electrophile and oxidant damage of mitochondrial DNA leading to rapid evolution of homoplasmic mutations. Proc Natl Acad Sci U S A. 2003; 100:1838–43. [PubMed: 12578990]

Melov S. Modeling mitochondrial function in aging neurons. Trends Neurosci. 2004; 27:601–6. [PubMed: 15374671]

Mittag TW, et al. Retinal damage after 3 to 4 months of elevated intraocular pressure in a rat glaucoma model. Invest Ophthalmol Vis Sci. 2000; 41:3451–9. [PubMed: 11006238]

Moreno MC, et al. Retinal oxidative stress induced by high intraocular pressure. Free Radic Biol Med. 2004; 37:803–12. [PubMed: 15384194]

Munemasa Y, et al. Protective effect of thioredoxins 1 and 2 in retinal ganglion cells after optic nerve transection and oxidative stress. Invest Ophthalmol Vis Sci. 2008; 49:3535–43. [PubMed: 18441302]

Munemasa Y, et al. Modulation of mitochondria in the axon and soma of retinal ganglion cells in a rat glaucoma model. J Neurochem. 2010; 115:1508–19. [PubMed: 20950337]

Olson VG, et al. Role of noradrenergic signaling by the nucleus tractus solitarius in mediating opiate reward. Science. 2006; 311:1017–20. [PubMed: 16484499]

Osborne NN. Mitochondria: Their role in ganglion cell death and survival in primary open angle glaucoma. Exp Eye Res. 2010; 90:750–7. [PubMed: 20359479]

Osborne NN, del Olmo-Aguado S. Maintenance of retinal ganglion cell mitochondrial functions as a neuroprotective strategy in glaucoma. Curr Opin Pharmacol. 2013; 13:16–22. [PubMed: 22999653]

Pascale A, et al. Protecting the retinal neurons from glaucoma: lowering ocular pressure is not enough. Pharmacol Res. 2012; 66:19–32. [PubMed: 22433276]

Pickrell AM, et al. The striatum is highly susceptible to mitochondrial oxidative phosphorylation dysfunctions. J Neurosci. 2011a; 31:9895–904. [PubMed: 21734281]

Pickrell AM, et al. Striatal dysfunctions associated with mitochondrial DNA damage in dopaminergic neurons in a mouse model of Parkinson's disease. J Neurosci. 2011b; 31:17649–58. [PubMed: 22131425]

Rana M, et al. An out-of-frame cytochrome b gene deletion from a patient with parkinsonism is associated with impaired complex III assembly and an increase in free radical production. Ann Neurol. 2000; 48:774–81. [PubMed: 11079541]

Reeve A, et al. The impact of pathogenic mitochondrial DNA mutations on substantia nigra neurons. J Neurosci. 2013; 33:10790–801. [PubMed: 23804100]

Rosca MG, et al. Glycation of mitochondrial proteins from diabetic rat kidney is associated with excess superoxide formation. Am J Physiol Renal Physiol. 2005; 289:F420–30. [PubMed: 15814529]

Santos JH, et al. Quantitative PCR-based measurement of nuclear and mitochondrial DNA damage and repair in mammalian cells. Methods Mol Biol. 2006; 314:183–99. [PubMed: 16673882]

Santos JM, et al. Mitochondrial biogenesis and the development of diabetic retinopathy. Free Radic Biol Med. 2011; 51:1849–60. [PubMed: 21911054]

Schärer OD, Jiricny J. Recent progress in the biology,chemistry and structural biology of DNA glycosylases. Bioessays. 2001; 23:270–281. [PubMed: 11223884]

Schon EA, et al. Human mitochondrial DNA: roles of inherited and somatic mutations. Nat Rev Genet. 2012; 13:878–90. [PubMed: 23154810]

Szczepanowska J, et al. Effect of mtDNA point mutations on cellular bioenergetics. Biochim Biophys Acta. 2012; 1817:1740–6. [PubMed: 22406627]

Tewari S, et al. Damaged mitochondrial DNA replication system and the development of diabetic retinopathy. Antioxid Redox Signal. 2012; 17:492–504. [PubMed: 22229649]

Tezel G. Oxidative stress in glaucomatous neurodegeneration: mechanisms and consequences. Prog Retin Eye Res. 2006; 25:490–513. [PubMed: 16962364]

Tezel G, Wax MB. Increased production of tumor necrosis factor-alpha by glial cells exposed to simulated ischemia or elevated hydrostatic pressure induces apoptosis in cocultured retinal ganglion cells. J Neurosci. 2000; 20:8693–700. [PubMed: 11102475]

Trifunovic A, et al. Somatic mtDNA mutations cause aging phenotypes without affecting reactive oxygen species production. Proc Natl Acad Sci U S A. 2005; 102:17993–8. [PubMed: 16332961]

Trifunovic A, et al. Premature ageing in mice expressing defective mitochondrial DNA polymerase. Nature. 2004; 429:417–23. [PubMed: 15164064]

Urcola JH, et al. Three experimental glaucoma models in rats: comparison of the effects of intraocular pressure elevation on retinal ganglion cell size and death. Exp Eye Res. 2006; 83:429–37. [PubMed: 16682027]

Vermulst M, et al. Quantification of random mutations in the mitochondrial genome. Methods. 2008; 46:263–8. [PubMed: 18948200]

Vives-Bauza C, Przedborski S. Mitophagy: the latest problem for Parkinson's disease. Trends Mol Med. 2011; 17:158–65. [PubMed: 21146459]

Wallace DC. Mitochondrial diseases in man and mouse. Science. 1999; 283:1482–8. [PubMed: 10066162]

Wang AL, et al. Age-related increase in mitochondrial DNA damage and loss of DNA repair capacity in the neural retina. Neurobiol Aging. 2010; 31:2002–10. [PubMed: 19084291]

Wax MB, et al. Induced autoimmunity to heat shock proteins elicits glaucomatous loss of retinal ganglion cell neurons via activated T-cell-derived fas-ligand. J Neurosci. 2008; 28:12085–96. [PubMed: 19005073]

Wu J, et al. Neuroprotective effect of upregulated sonic Hedgehog in retinal ganglion cells following chronic ocular hypertension. Invest Ophthalmol Vis Sci. 2010; 51:2986–92. [PubMed: 20071678]

Yakes FM, Van Houten B. Mitochondrial DNA damage is more extensive and persists longer than nuclear DNA damage in human cells following oxidative stress. Proc Natl Acad Sci U S A. 1997; 94:514–9. [PubMed: 9012815]

Yang L, et al. Role of dorsomedial hypothalamic neuropeptide Y in modulating food intake and energy balance. J Neurosci. 2009; 29:179–90. [PubMed: 19129396]

Yao J, et al. Inhibition of amyloid-beta (Abeta) peptide-binding alcohol dehydrogenase-Abeta interaction reduces Abeta accumulation and improves mitochondrial function in a mouse model of Alzheimer's disease. J Neurosci. 2011; 31:2313–20. [PubMed: 21307267]

Yu-Wai-Man P, et al. Mitochondrial optic neuropathies - disease mechanisms and therapeutic strategies. Prog Retin Eye Res. 2011; 30:81–114. [PubMed: 21112411]

Zhang Q, et al. Circulating mitochondrial DAMPs cause inflammatory responses to injury. Nature. 2010; 464:104–7. [PubMed: 20203610]

Zhang SH, et al. Distinctive gene transduction efficiencies of commonly used viral vectors in the retina. Curr Eye Res. 2008; 33:81–90. [PubMed: 18214745]

Highlights

1. Progressive RGC loss after transiently high intraocular pressure (IOP)
2. Cumulative mtDNA damage and mutations occurs in RGCs after IOP elevation
3. mtDNA damage and mutations result in RGC apoptosis
4. mtDNA alterations increase the vulnerability of RGC to high IOP and glutamate level
5. Preventing mtDNA alterations improves RGC survival in glaucomatous rat model

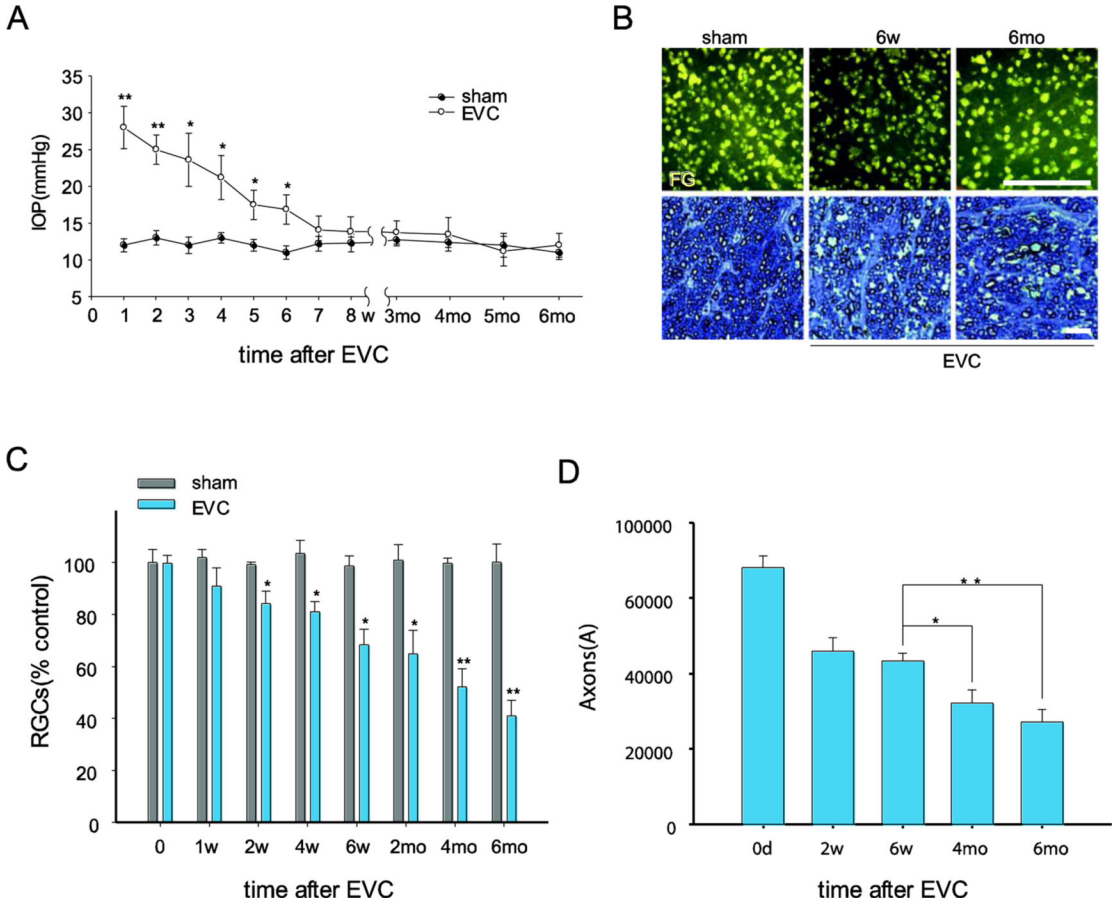

Fig. 1.

EVC-induced IOP elevation leads to a progressive loss of RGCs and their axons, even after the IOP has returned to normal levels. ***A***, Time course of IOP after EVC (*n*=40/time point). IOP elevation was observed at 1 day and was sustained for 6 weeks after EVC treatment. ***B***, Representative photographs of FG-labeled RGCs in flat-mounted retinas (top panels, scale bar, 100 μm) and toluidine blue staining of optic nerve cross-sections (bottom panels, scale bar, 100 μm). ***C***, ***D***, Quantitation of FG-labeled RGCs (***C***) and axons in the optic nerve (***D***) in EVC-treated eyes during IOP elevation and after return of the IOP to normal levels (n=8/time point). The values are the means ± SEMs. **p*<0.05 and ** *p*<0.01 compared with the contralateral sham operation control eye. EVC: episcleral vein cauterization. w: week, mo: month.

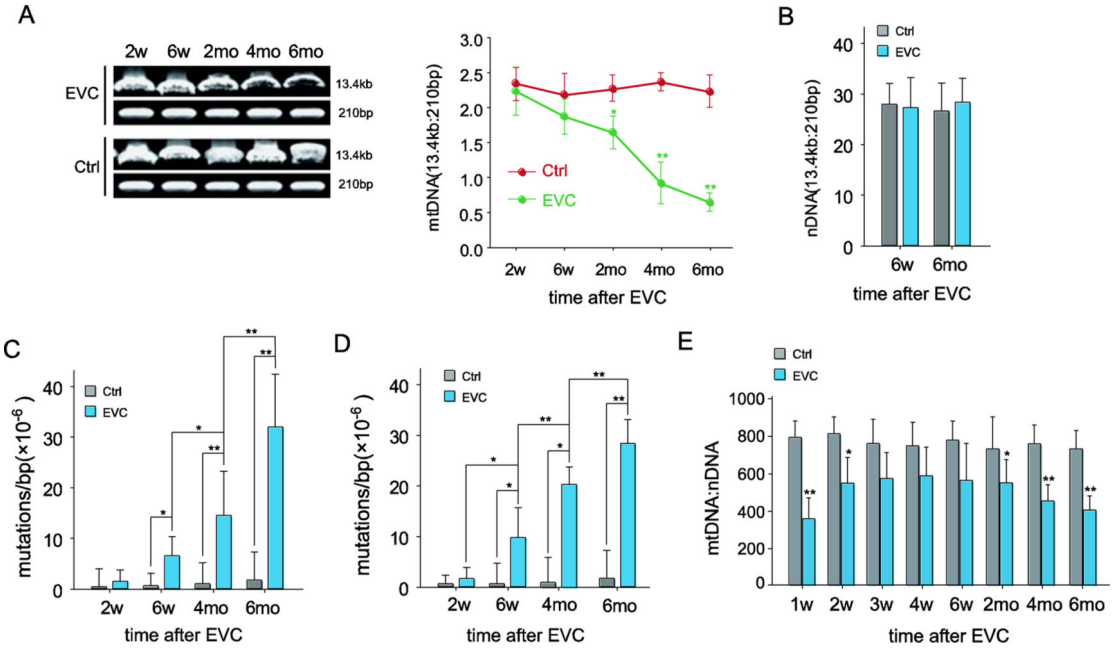

Fig. 2.

The mtDNA changed following IOP elevation. ***A***, mtDNA damage, which was evaluated by the ratio of 13.4-kb and 210-bp using LX-PCR, increased after EVC. The PCR products were analyzed by electrophoresis in an agarose gel (right panel), and the ratios of the long/short amplicons were calculated (left panel). ***B***, The ratios of the long/short amplicons demonstrating no significant nDNA damage after high IOP. ***C***, ***D***, Quantification of the point mutation frequency per base pair at 1,427 (C) and 8,335 (D) sites by the random mutation capture assay. ***E***, Quantitative analysis of mtDNA copy number per nuclear genome. *n*=24/time point/group. The values are the means ± SEMs. **p*<0.05, ** *p*<0.01 compared with the contralateral sham-operated control. EVC: episcleral vein cauterization. Ctrl: contralateral sham operation control.

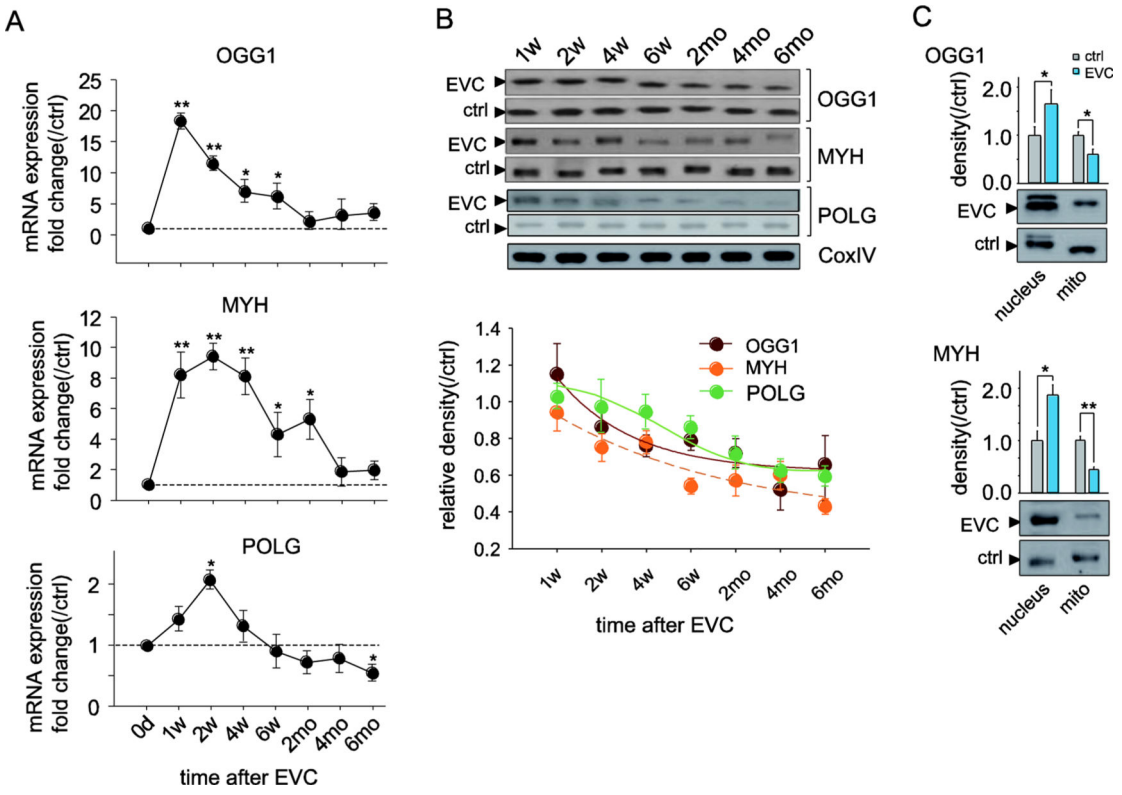

Figure 3.

Dynamic profile of the expression of mtDNA repair/replication enzymes in the RGCs of EVC eyes. ***A***, Real-time PCR analysis of the gene expression of *OGG1*, *MYH*, and *POLG* in isolated RGCs. The fold change relative to contralateral sham operation controls was calculated using the ΔΔCt method. ***B***, Western blotting analysis showing that the protein expression of OGG1, MYH, and POLG in the mitochondria of RGCs decreased after high IOP. CoxIV was used as an internal reference. The data are expressed as normalized ratios (Ctrl = 1). ***C***, Western blots demonstrating the disparity in OGG1 and MYH protein expression in the mitochondria and in the nucleus 6 months after EVC. For each, the values are the means ± SEMs (n=22–24 retinas/group). *p<0.05, **p<0.01 compared with the contralateral sham operation control. mito: mitochondria. w: week, mo: month.

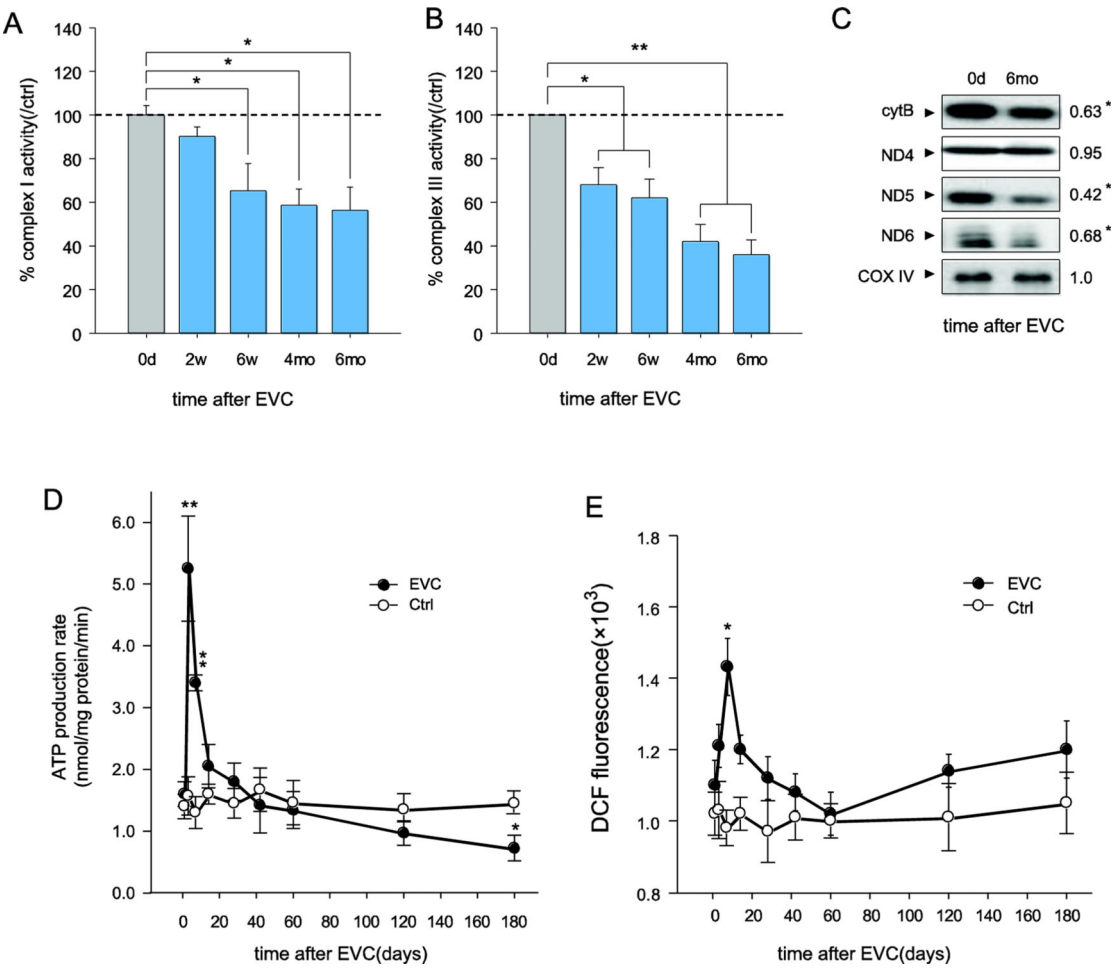

Fig. 4.

Accelerated mitochondrial dysfunction in the RGCs of EVC eyes, even after the reversal of IOP elevation. ***A***, ***B***, Complex I and III activities in the mitochondria of isolated RGCs decreased after EVC by measuring the consumption of NADH at 340 nm for complex I (***A***) and the reduction of cytochrome C at 550 nm for complex III (***B***). Values for the mitochondria of RGCs from the contralateral sham-operated control were set at 100%. ***C***, Quantitative analysis of the mtDNA-encoded proteins ND4, ND5, ND6 and cytochrome b by western blot. CoxIV was used as a control. The value is the 6 month/0 day band density ratio. ***D***, The ATP production rate in mitochondria isolated from RGCs was analyzed using a luciferase-based assay. ***E***, The ROS concentrations in the RGCs were measured with the dye *DCFH-DA*. The values are the means ± SEMs. *$p<0.05$, ** $p<0.01$ compared to the contralateral sham operation control. RGCs isolated from 7-8 retinas were pooled to obtain 1 sample, and 3 samples (n=21–24) were used for each time point per group.

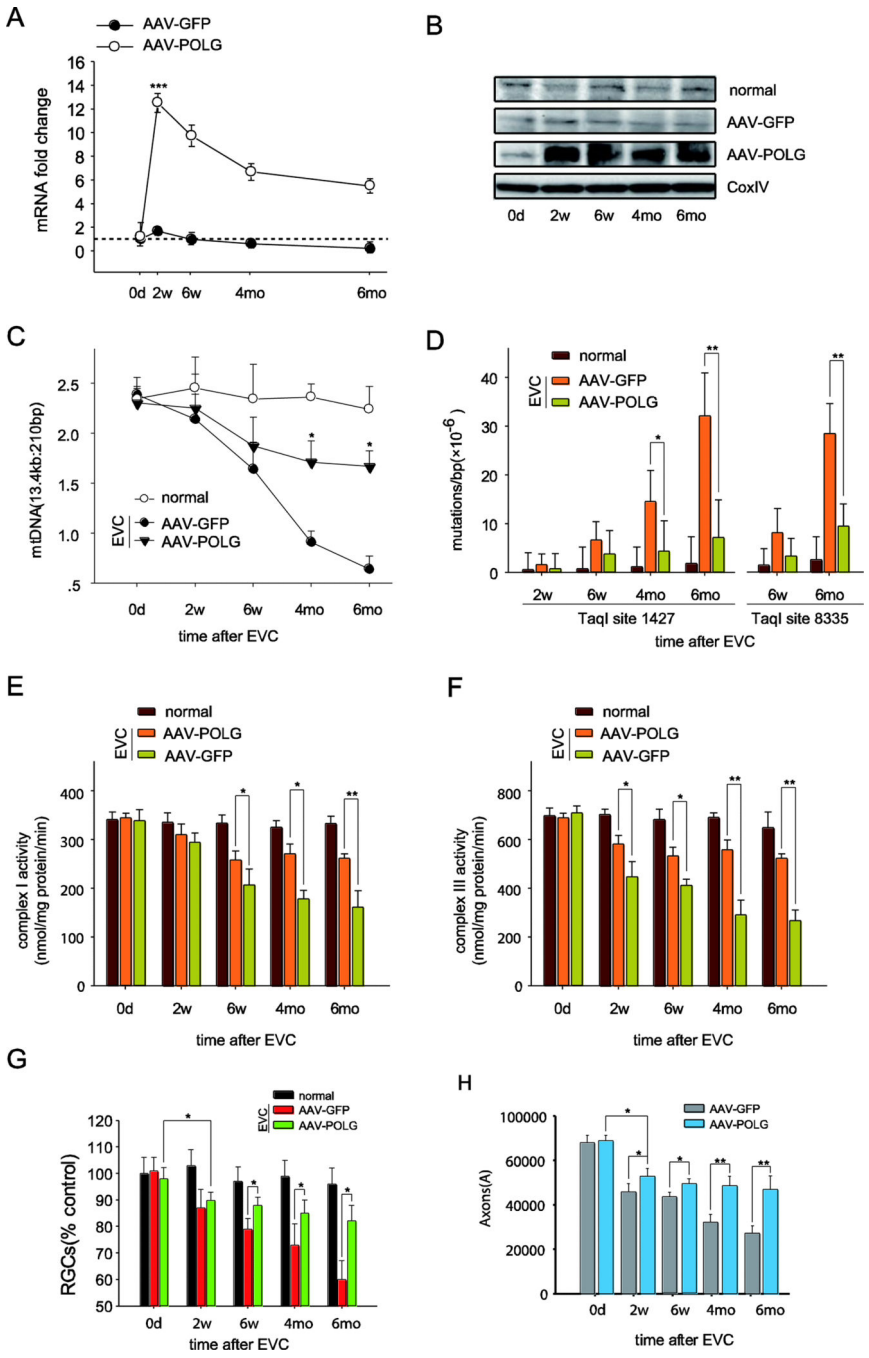

Fig. 5.

Intravitreal injection of AAV2-POLG prevented mtDNA alterations and promoted RGC survival in the rat glaucomatous model. ***A***, POLG mRNA levels in the isolated RGCs were quantified by real-time PCR at 0 days, 2 weeks, 6 weeks, 4 months, and 6 months after EVC with AAV2-POLG/GFP. The fold change relative to normal age-matched controls was calculated using the $\Delta\Delta C_t$ method. ***B***, The mitochondrial protein levels of POLG in the RGCs were detected by western blot at different time points after EVC with AAV2-POLG/GFP. CoxIV was used as an internal reference. ***C***, The mitochondrial DNA damage in the

isolated RGCs was determined by LX-PCR after EVC with AAV2-POLG/GFP. ***D***, The random mutation capture assay revealed that the point mutation frequency in mtDNA decreased at either position 1,427 or 8,335 of the mitochondrial genome after EVC with AAV2-POLG/GFP. ***E***, ***F***, The measurement of complex I (***E***) and III (***F***) activities in mitochondria isolated from RGCs at different times after EVC with AAV2-POLG/GFP. ***G***, ***H***, Quantitation of DiI-labeled RGCs (G) and toluidine blue-stained axons (H) showed that RGCs and their axon survival increased in EVC-treated eyes with AAV2-POLG compared to those with AAV2-GFP. *n*=24 retinas/time point/group (A, B, C, D). *n*=21–23/ time point/ group (E, F). *n*=6/ time point/group (G, H).

For each, the values are the means ± SEMs. **p*<0.05, ** *p*<0.01 and ****p*<0.001 compared with the EVC-treated eyes with AAV2-GFP. normal: age-matched normal control. EVC: episcleral vein cauterization. w: week, mo: month.

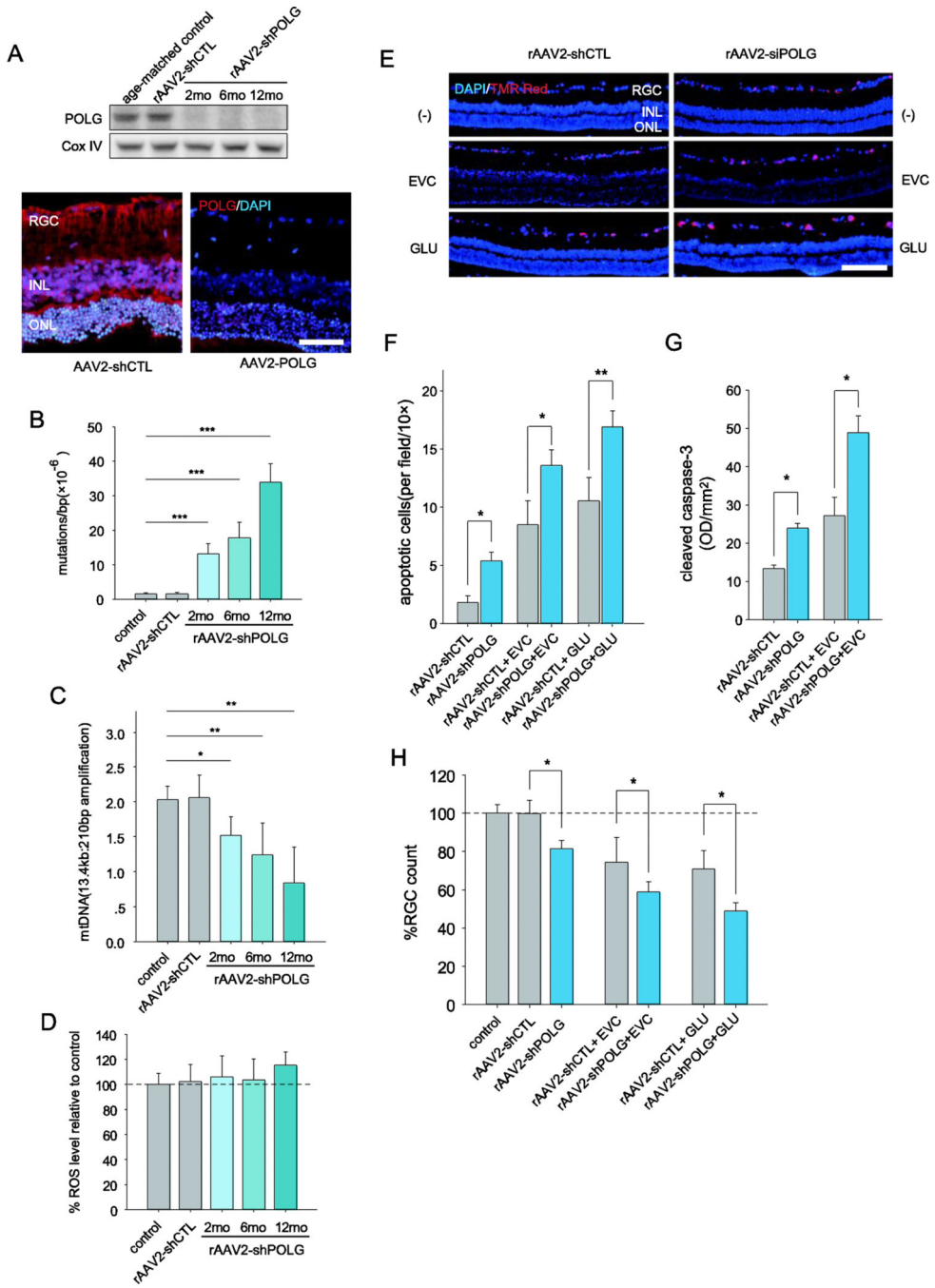

Fig. 6.

RGCs with increased mtDNA damage and mutations are not only prone to apoptosis but also have an increased vulnerability to IOP or glutamate challenge. ***A***, Western blot analysis of POLG expression in the mitochondria of RGCs after AAV-shPOLG treatment (upper panel). Immunofluorescence staining showed POLG expression increased at 1 year after intravitreal injection of AAV2-shPOLG (lower panel). Red: POLG; blue: DAPI. Scale bar: 50 μm. ***B***, ***C***, Quantitative analysis of mtDNA mutations at position 8,335 of mtDNA (**B**) and damage (**C**) in RGCs after intravitreal injection of AAV-shPOLG using random

mutation capture assay and LX-PCR, respectively. ***D***, The ROS levels in isolated RGCs were determined using *DCFH-DA* dye. The values are expressed as percentages, with the values of the age-matched controls set at 100%. ***E***, A TUNEL assay was used with in situ retinas to detect apoptotic cell death. Representative microscopic images showing TUNEL-positive cells in the retinas treated with AAV2-shPOLG alone; AAV2-shPOLG and EVC/glutamate; AAV2-shCTL alone; and AAV2-shCTL and EVC/glutamate. Red: TUNEL positive; blue: DAPI. Scale bars, 100 μm. ***F***, Quantitative analysis of RGC apoptosis determined by TUNEL assay. The data are expressed as apoptotic cell counts. ***G***, Determination of caspase-3 activation using an antibody to cleaved caspase-3 by western blot. The values were expressed as arbitrary OD units per unit area (OD/mm^2) using ImageJ software. ***H,*** Quantitation of DiI-labeled RGCs in age-matched controls and those treated with AAV2-shPOLG alone; AAV2-shPOLG and EVC/glutamate; AAV2-shCTL alone; and AAV2-shCTL and EVC/glutamate. The data are presented as percentages, with the values from the age-matched controls set at 100%. All values in these figures are presented as the means ± SEMs, *$p<0.05$, ** $p<0.01$ ($n=18–21$ retinas/time point/group). EVC: episcleral vein cauterization. GLU: glutamate.